

HADRONIC TRANSPORT MODEL WITH A PHASE TRANSITION*

P. DANIELEWICZ¹, P.-B. GOSSIAUX^{1,2} AND R. A. LACEY³

¹*National Superconducting Cyclotron Laboratory
and the Department of Physics and Astronomy, Michigan State
University, East Lansing, MI 48824-1321, USA*

²*SUBATECH, Ecole des Mines, F-44070 Nantes, France*

³*Departments of Chemistry and Physics, State University of
New York at Stony Brook, Stony Brook, NY 11794-3400, USA*

Abstract. We specify a tractable transport model with thermodynamic properties close to those expected for the strongly interacting matter. In particular, at high temperatures, the matter undergoes a phase transition, such as to the quark-gluon plasma, with a drop in masses of elementary excitations and a rapid increase in the number of degrees of freedom. We show that a softening of the equation of state such as associated with the transition to quark-gluon plasma should be observable in the elliptic-flow excitation function from heavy-ion reactions.

1. Introduction

One of the important goals of the heavy-ion reaction studies is the detection of quark-gluon (QG) plasma. Reaching the transition to QG plasma requires a significant increase in hadron density in a reaction, through an increase in baryon density, or an increase in temperature, or both. General expectations concerning the approach to the transition are as follows. When hadrons increase in density in some spatial region, they push out the standard nonperturbative vacuum. The fraction of the volume taken by the nonperturbative vacuum decreases and this, on the average, reduces hadron

*Talk given at the Workshop on Nuclear Matter in Different Phases and Transitions, Les Houches, March 31 – April 10, 1998.

masses associated with the condensate in that vacuum. At the transition, the masses of elementary excitations, now quarks and gluons, drop to values close to zero. The number of the degrees of freedom at the phase transition dramatically increases.

Specific quantitative information on the transition to QG plasma comes from numerical quantum-chromodynamic lattice calculations. Since these results pertain to a baryonless system at equilibrium, though, they are insufficient for the *reaction description*. The relatively well understood domain is that of the strongly interacting matter at low energy densities. That matter is describable in terms of individual hadrons scattering on each other, with cross sections close to those in free space. The hadrons further feel the overall mean field produced by remaining hadrons in the vicinity. Transport theory based on such concepts had much success with low and intermediate energy reactions. Ground-state properties of nuclear matter are rather well known. The areas of most uncertainty regarding the strongly-interacting matter include the QG plasma out of equilibrium. The conversion of the plasma into hadrons is not comprehended. One can suspect that somehow the characteristic hadronic distances and time-scales are involved.

The need to test for the presence of the phase transition in reactions and the difficult theoretic situation described above lead us to consider a dynamic hadronic model for reactions, consistent with all known limits such as low-density hadron matter and the thermal equilibrium at baryon chemical potential $\mu = 0$. The model could be, otherwise, applied in general nonequilibrium situations. In the simplest possible model, the particle masses would be reduced by one common factor in connection with the phase transition:

$$m_0 \rightarrow m = m_0 S. \quad (1)$$

The mass reduction factor S should tend to zero as particle density increases. Physically, as the particle density increases, the particles present in a certain region may start to overlap with each other. Overcounting of the degrees of freedom could be treated in terms of excluded volume nonrelativistically, but no similar simple and consistent procedure exists relativistically. Relying on the fact that the number of effective degrees of freedom should not exceed the number of fundamental degrees of freedom, we decided to adopt a cutoff in the mass spectrum of the included hadrons to roughly match the number of quarks and gluons, and disregard the excluded volume. Thus, the number of quarks and gluons is $24 + 16 = 40$. We include nucleons, deltas, and their antiparticles, pions and ρ mesons. When these particles become massless, we roughly match the number of massless degrees of freedom in the plasma, with $8 + 32 + 3 + 9 = 52$, expecting a sensible increase in the entropy and in other thermodynamic quantities across the transition.

For the selected degrees of freedom, one needs to specify a dynamics. At low energies, the combination of collisions and mean field was successful; the mean field could be used to lower masses. The common approach is to start from a Lagrangian and adopt a mean-field approximation to resulting equations of motion. The mean field often then has undesirable properties and, to repair these, more and more nonlinear terms are added the Lagrangian making it cumbersome. We decided to circumvent these steps by formulating our approach within the relativistic Landau theory.

2. Relativistic Landau Theory

Within the Landau theory, the interactions are specified by giving the energy density as a functional of particle phase-space distributions f [1]

$$T^{00} = e \equiv e\{f\}. \quad (2)$$

The single-particle energies represent functional derivatives of the energy

$$\epsilon_{\mathbf{p}}^i = \frac{\delta e}{\delta f^i(\mathbf{p}, \mathbf{r}, t)}, \quad (3)$$

where i is the particle index. The single-particle energy and momentum, $(\mathbf{p}, \epsilon_{\mathbf{p}})$, transform, generally, as a four-vector.

In the simplest parametrization of the energy, ensuring covariance, the net energy consists of the sum of kinetic energies and corrections for interactions dependent on scalar and vector densities:

$$e = \sum_i \int d\mathbf{p} \epsilon_{\mathbf{p}}^i f^i(\mathbf{p}) + e_s(\rho_s) + e_v(\rho_v), \quad (4)$$

in a local frame, with

$$\rho_s = \sum_i \int d\mathbf{p} \frac{m^i m_0^i}{\sqrt{m^{i2} + p^2}} f^i(\mathbf{p}) \quad (5)$$

and

$$\rho_v = \sum_i B^i \int d\mathbf{p} f^i(\mathbf{p}). \quad (6)$$

Dependence on two densities, ρ_s and ρ_v , is needed to parametrize, independently, the thermodynamic properties along the $\mu = 0$ and $T = 0$ axes.

Contributions of different hadrons to the scalar density are weighted with the hadron mass, to ensure that the masses change by the common factor S ,

$$m^i = m_0^i S(\rho_s), \quad \text{where} \quad S = \int \frac{d\rho_s}{\rho_s} \frac{de_s}{d\rho_s}. \quad (7)$$

The single-particle energy in a local rest frame is then

$$\epsilon_{\mathbf{p}}^i = \sqrt{m^{i2} + p^2} + B^i V(\rho_v), \quad \text{with } V = \int \frac{d\rho_v}{\rho_v} \frac{de_v}{d\rho_v}. \quad (8)$$

In any frame, the baryon four-current is

$$\rho_v^\mu = \left(\sum_i \int d\mathbf{p} f^i, \sum_i \int d\mathbf{p} \frac{\partial \epsilon^i}{\partial \mathbf{p}} f^i \right), \quad (9)$$

and $\rho_v^\mu \rho_{v\mu} = \rho_v^2$. The canonical four-momentum p^μ may be expressed, similarly to electrodynamics, in terms of the kinematic four-momentum $p^{*\mu}$ and the four-vector potential in the direction of the four-current,

$$p^{i\mu} = p^{i*\mu} + B^i V \rho_v^\mu / \rho_v, \quad (10)$$

with $p^{i*2} = m^{i2}$. Locally, the canonical and kinematic three-momenta are identical, $\mathbf{p}^{i*} = \mathbf{p}^i$.

Now we move on to the thermodynamic properties of matter. Our results for equilibrium generalize those found within the Walecka model.

3. Thermodynamic Properties

The transition to QG plasma is characterized by an increase in the number of the degrees of freedom and by a decrease in the masses of elementary quanta. In the discussed model, the transition may be produced by requiring the drop of masses with an increase in density. The decrease in masses should lead to an additional increase in the number of particles present at a given T and, in turn, to an additional decrease in the masses. Eventually, as T grows the system may become unstable and a phase transition can take place.

In assessing whether or not the phase transition takes place, it is first necessary to determine what mass reduction is reached at any T . In the model, the dependence $S(\rho_s)$ is prescribed; at low ρ_s , $S \simeq 1 - a \rho_s$, with $a > 0$, given the considerations before. Besides, the consistency condition, from the definition of the density, must be met at a given T :

$$\begin{aligned} \rho_s &\equiv \rho_s(S, T) \\ &= \sum_i \int d\mathbf{p} \frac{m_0^{i2} S}{\sqrt{m_0^{i2} S^2 + p^2}} \frac{1}{\exp\left(\sqrt{m_0^{i2} S^2 + p^2}/T\right) \pm 1}, \quad (11) \end{aligned}$$

where the equilibrium form of f was inserted. The two equations give ρ_s and S for a given T , as schematically illustrated for the Walecka model in Fig. 1

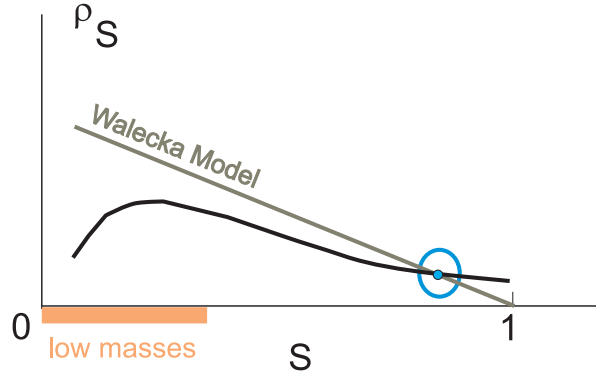


Figure 1. The values of ρ_s and S at a given T are found in the $\rho_s - S$ plot from crossing of the lines given by the $S(\rho_s)$ dependence (straight line in the Walecka model) and by the consistency relation (line with the hump).

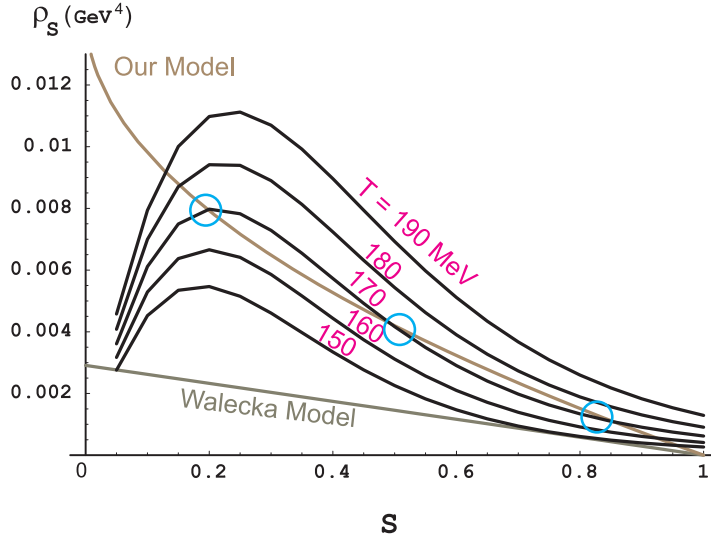


Figure 2. Three crossings of the $S(\rho_s)$ line with the $\rho_s(S, T)$ line indicate the presence of a phase transition.

displaying a $\rho_s - S$ plot. The values are found from the crossing of the lines given by (11) and by $S(\rho_s)$. The second of the dependencies is linear in the Walecka model at all ρ_s . At sufficiently low T , only one crossing is found but, as T grows, the hump in the curve from the consistency relation grows. Eventually, three crossings may be found, as shown in Fig. 2, indicating the presence of a phase transition. In the Walecka model the interactions are very strong:

$$S = 1 - 2.6 (\text{fm}^3/\text{GeV}) \rho_s, \quad (12)$$

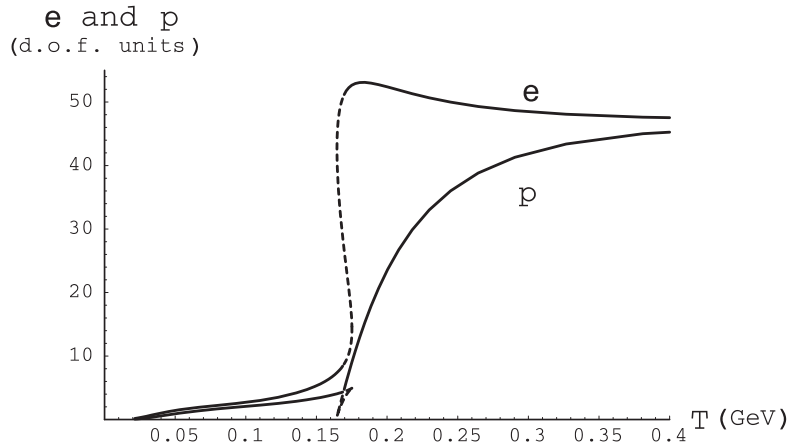


Figure 3. Energy density e and pressure p , scaled by the factors $\pi^2 T^4/30$ and $\pi^2 T^4/90$, respectively, as a function of T .

and the phase transition takes place at low temperatures $T < 100$ MeV. We use a weaker dependence of S on ρ_s ,

$$S = (1 - 0.54 (\text{fm}^3/\text{GeV}) \rho_s)^2, \quad (13)$$

getting the phase transition at $T \approx 170$ MeV as found in lattice calculations [2]. Figure 3 displays the energy density e and pressure p as a function of T at $\mu = 0$ in our model, divided by the customary factors of $\pi^2 T^4/30$ and $\pi^2 T^4/90$, respectively, to show the effective number of degrees of freedom. A characteristic knot is seen in $p(T)$ indicating the transition. Qualitative features found in the lattice calculations [2] are reproduced naturally within the model, such as the rapid rise of e across the transition region and a slow rise of p . Having set the thermodynamic properties at $\mu = 0$, we turn to the properties at $T = 0$.

At $T = 0$ the energy per baryon e/ρ_v should have a minimum of $939 - 16$ MeV, at $\rho_v = \rho_0 = 0.16 \text{ fm}^{-3}$, with the curvature characterized by the incompressibility $K \simeq 210$ MeV. For some prescribed dependence $V(\rho_v)$, the density ρ_v and the potential V , at a given μ , may be found with the help of the consistency relation:

$$\rho_v \equiv \rho_v(V) = \sum_i B^i \int d\mathbf{p} \theta \left(\mu - \sqrt{m^2 + p^2} - B^i V \right). \quad (14)$$

The values can be found from a crossing of the lines in a $\rho_v - V$ plane. Note that the already set $S(\rho_s)$ enters into (14). Three rather than one

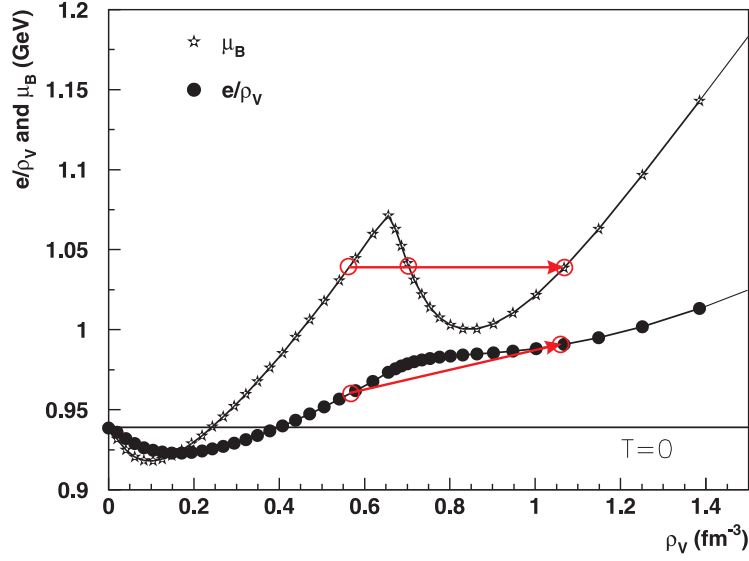


Figure 4. Chemical potential μ and energy per baryon e/ρ_v at $T = 0$ as a function of ρ_v . The high-density phase transition is indicated with arrows.

crossing in the $\rho_v - V$ plane indicate a phase transition. We take V out of a combination of powers, exclusively repulsive,

$$V = \frac{a (\rho_v / \rho_{v0})^2}{1 + b \rho_v / \rho_{v0} + c (\rho_v / \rho_{v0})^{5/3}}, \quad (15)$$

and adjust the parameters to reproduce the ground-state nuclear-matter properties. We find $a = 146.32$ MeV, and $b = 0.4733$. The value of $c = 51.48$ and the power in the term that c multiplies are fixed by the requirement that the equation of state of a free quark gas is reproduced [3] at high ρ_v . With these parameters we find a first-order phase transition at $T = 0$, see Fig. 4, taking the system from $\rho_v \sim 3.5 \rho_0$ to $\rho_v \sim 7 \rho_0$. The phase transition is fragile, i.e. moderate changes in the parameters replace the phase transition by a transitional behavior. In any case, though, the matter exhibits a rapid change of properties along the $T = 0$ axis above $3 \rho_0$. The masses drop rapidly as the scalar density increases. This behavior reflects that along the $\mu = 0$ axis.

When we consider all possible values of μ and T , we find the phase transitions only in the vicinity of $\mu = 0$ and $T = 0$ axes. For moderate values of μ and T , rather than going through a phase transition, the matter exhibits only a transitional behavior. This is illustrated with Fig. 5 that shows the mass reduction factor S as a function of both μ and T . At high

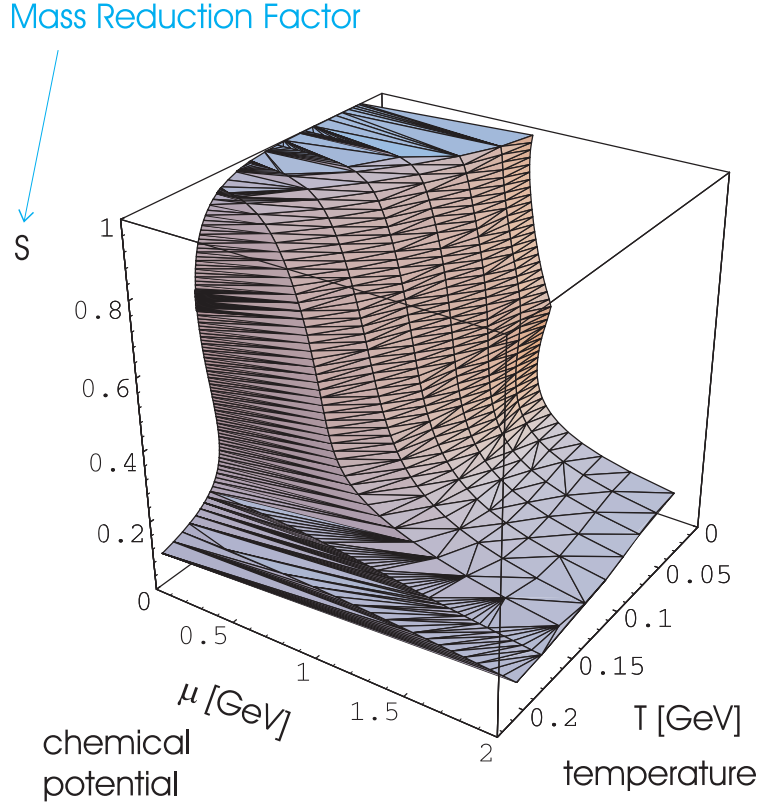


Figure 5. Mass reduction factor S as a function of chemical potential μ and temperature T .

temperatures and/or baryon densities, the masses fall to 20% or less of vacuum values.

4. Transport Theory

Consistently with (2), the spatial and temporal changes in the phase-space distribution functions are described by the Boltzmann equation

$$\frac{\partial f}{\partial t} + \frac{\partial \epsilon_{\mathbf{p}}}{\partial \mathbf{p}} \frac{\partial f}{\partial \mathbf{r}} - \frac{\partial \epsilon_{\mathbf{p}}}{\partial \mathbf{r}} \frac{\partial f}{\partial \mathbf{p}} = I, \quad (16)$$

which has the same general form relativistically as nonrelativistically. On the l.h.s. of (16), $\partial \epsilon_{\mathbf{p}} / \partial \mathbf{p}$ is the velocity and $-\partial \epsilon_{\mathbf{p}} / \partial \mathbf{r}$ is force, while I on the r.h.s. is the collision integral. In terms of kinematic variables, the Boltzmann

equation acquires a simple form:

$$\frac{\partial f}{\partial t} + \frac{\mathbf{p}^*}{\epsilon_{\mathbf{p}}^*} \frac{\partial f}{\partial \mathbf{r}} - \frac{\partial}{\partial \mathbf{r}} (\epsilon_{\mathbf{p}}^* + V^0) \frac{\partial f}{\partial \mathbf{p}^*} = I. \quad (17)$$

This result generalizes the one obtained by Ko *et al.* [4] within the Walecka model. The gradient in the force in (17) does not just act on the potential, since the kinetic energy depends on position through mass.

Collisions can, generally, change the particle number and, thus, the integral is:

$$\begin{aligned} \gamma_1 I &= \sum_{n, n' \geq 2} \int \frac{d\mathbf{p}_2}{\gamma_2} \dots \frac{d\mathbf{p}_n}{\gamma_n} \int \frac{d\mathbf{p}'_1}{\gamma'_1} \dots \frac{d\mathbf{p}'_{n'}}{\gamma'_{n'}} |\mathcal{M}|^2 \\ &\quad \times \delta \left(\sum_{i'=1}^{n'} p_{i'} - \sum_{i=1}^n p_i \right) (f'_1 \dots f'_{n'} - f_1 \dots f_n) \\ &= \sum_{n, n' \geq 2} \int \frac{d\mathbf{p}_2^*}{\gamma_2} \dots \frac{d\mathbf{p}_n^*}{\gamma_n} \int \frac{d\mathbf{p}'_1^*}{\gamma'_1} \dots \frac{d\mathbf{p}'_{n'}^*}{\gamma'_{n'}} |\mathcal{M}|^2 \\ &\quad \times \delta \left(\sum_{i'=1}^{n'} p_{i'}^* - \sum_{i=1}^n p_i^* \right) (f'_1 \dots f'_{n'} - f_1 \dots f_n) \end{aligned} \quad (18)$$

where n and n' are particle numbers in the initial and final states. The rate for collisions is proportional to the respective matrix-element squared, energy and momentum are conserved in the collisions, and the rate of change in the occupation results from the difference in gain and loss. The statistics is suppressed in (18). Since, locally, canonical momenta differ from kinematic momenta by a constant shift, the collision integral acquires a particular simple form in the kinematic variables (18). Compared to vacuum, in the medium the mass scale just changes by the factor of S .

When aiming at a certain equation of state (EOS) in a calculation, it is essential to obey detailed balance relations for elementary collision processes. That is relatively straightforward for processes with at most two particles in the initial and final states, but difficult for processes with more particles. Given this, we adopt a compromise in our model, treating high- and low-energy processes differently. The elementary low-energy processes, that establish thermodynamic equilibrium, with at most two particles in any state, have a strictly enforced detailed balance. This is in contrast to the high-energy processes for which the inverse processes are less likely. The high-energy production processes are parametrized using experimental data on net cross sections, pion multiplicities, hadron rapidity, and transverse-momentum distributions. The concept of transverse-momentum

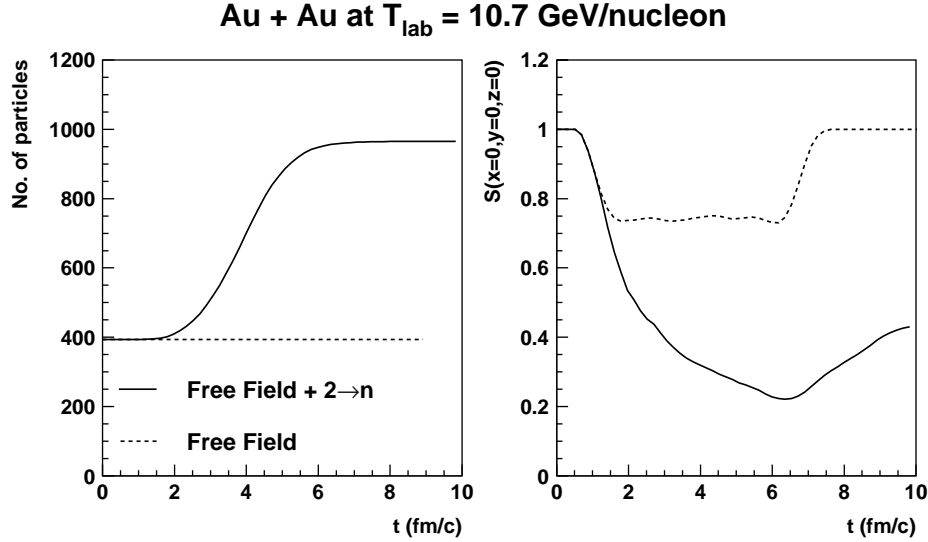


Figure 6. Evolution of the number of hadrons (left) and of the mass factor S at the system center (right) in $b = 0$ Au + Au reaction at 10.7 GeV/nucleon. Dashed lines show the evolution from the transport equation with mean field only and solid lines show evolution from the transport equation with mean field and collisions.

phase-space is followed, with a leading particle effect, in a similar manner to ARC [5],

$$\gamma I \propto \prod_{j=1}^N \frac{d\mathbf{p}'_j}{\gamma'_j} e^{-B E'_{\perp j}} W_{\parallel j} \times \delta \left(p_1 + p_2 - \sum_{j=1}^N p'_j \right). \quad (19)$$

The longitudinal weight is $W_{\parallel} = e^{-|y-y_i|}$ for leading particles and $W_{\parallel} = 1$ for central ones.

As to low-energy processes, we ensure that, besides elastic, we include all those needed for the chemical equilibration, i.e. $\pi + N \leftrightarrow \Delta$, $\pi + \Delta \leftrightarrow N + \rho$, $\pi + \pi \leftrightarrow \rho$, $\pi + \pi \leftrightarrow \rho + \rho$, $N + N \leftrightarrow N + \Delta$, $N + N \leftrightarrow \Delta + \Delta$, $N + \Delta \leftrightarrow \Delta + \Delta$, $B + \bar{B} \leftrightarrow \pi + \pi$, $B + \bar{B} \leftrightarrow \rho + \rho$, and $B + \bar{B} \leftrightarrow \rho + \pi$. The practical implementation of all the processes, though, is still not completed.

With only the high-energy processes in the model, we test whether the phase transition may be crossed in the heavy-ion reactions at AGS. Specifically, we examine the head-on reaction of Au + Au at 10.7 GeV/nucleon. Figure 6 shows, as a function of time, the net particle number and the mass reduction factor S at the center of that system evolved with the mean field only in the transport equation and with the mean field and the elementary collisions. In the case of mean field only, the masses drop to values comparable to those in normal nuclei and then recover. In the case with collisions,

the particle number increases by a factor of 2.5 compared to the initial state and masses at the center drop to values such as behind the transition in our model. After $t \sim 6$ fm/c in the latter evolution, the system appears to fragment into domains of low values of S surrounded by regions of values close to 1.

As the QGP phase transition appears to be crossed at AGS energies, we now turn to the experimental observables that could signal the crossing.

5. Elliptic Flow

Regions of transitional behavior and of phase transitions are commonly characterized by the changes in the speed of sound. At the first-order phase transition, such as in Figs. 3 and 4, the speed of sound, $c_s = \sqrt{\partial p / \partial e}$, vanishes. Above the phase transition in Fig. 3, the speed of sound remains low, due to the slower rise of pressure p with temperature than the rise of energy e . Also for the situation in Fig. 4, the speed of sound is low above the phase transition compared to the region below the transition.

A sensitive measure of the speed of sound or pressure compared to the energy density early on in the reactions is the elliptic flow. The elliptic flow is the anisotropy of transverse emission at midrapidity. At AGS energies, the elliptic flow results from a strong competition [6] between squeeze-out and in-plane flow, as illustrated in Fig. 7. In the early stages of the collision as shown in Fig. 7(b), the spectator nucleons block the path of participant hadrons emitted toward the reaction plane; therefore the nuclear matter is initially squeezed out preferentially orthogonal to the reaction plane. This squeeze-out of nuclear matter leads to negative elliptic flow. In the later stages of the reaction, as shown in Fig. 7(c), the geometry of the participant region (i.e. a larger surface area exposed in the direction of the reaction plane) favors in-plane preferential emission and hence positive elliptic flow.

The squeeze-out contribution to the elliptic flow and the resulting net sign of the flow depend on two factors: (i) the pressure built up in the compression stage compared to the energy density, and (ii) the passage time for removal of the shadowing due to the projectile and target spectators. In the hydrodynamic limit, the characteristic time for the development of expansion perpendicular to the reaction plane is $\sim R/c_s$, where the speed of sound is $c_s = \sqrt{\partial p / \partial e}$, R is the nuclear radius, p is the pressure and e is the energy density. The passage time is $\sim 2R/(\gamma_0 v_0)$, where v_0 is the c.m. spectator velocity. The squeeze-out contribution should then reflect the ratio [7]

$$\frac{c_s}{\gamma_0 v_0}. \quad (20)$$

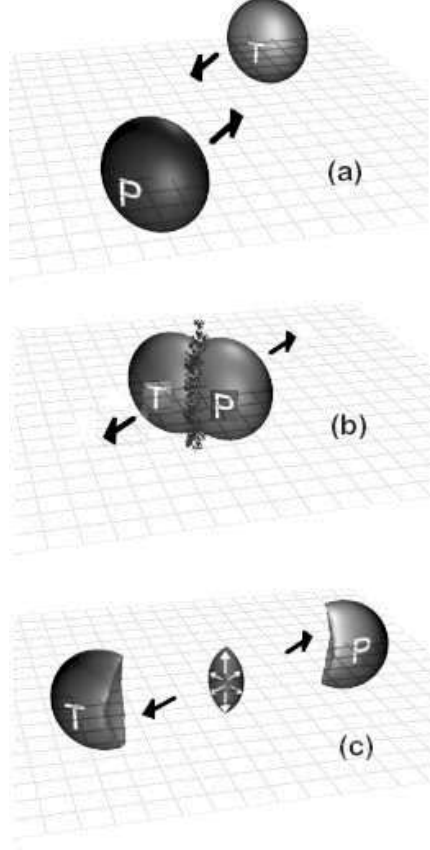


Figure 7. Schematic illustration of the collision of two Au nuclei at relativistic energies. Time shots are shown for an instant before the collision (a), early in the collision (b), and late in the collision (c).

According to (20) the squeeze-out contribution should drop with the increase in energy, because of the rise in v_0 and then in γ_0 . A stiffer EOS should yield a higher squeeze-out contribution. A rapid change in the stiffness with baryon density and/or excitation energy should be reflected in a rapid change in the elliptic flow excitation function. A convenient measure of the elliptic flow is the Fourier coefficient $\langle \cos 2\phi \rangle \equiv v_2$, where ϕ is the azimuthal angle of a baryon at midrapidity, relative to the reaction plane. When squeeze-out dominates, the Fourier coefficient is negative. When late-stage in-plane emission dominates, the coefficient is positive.

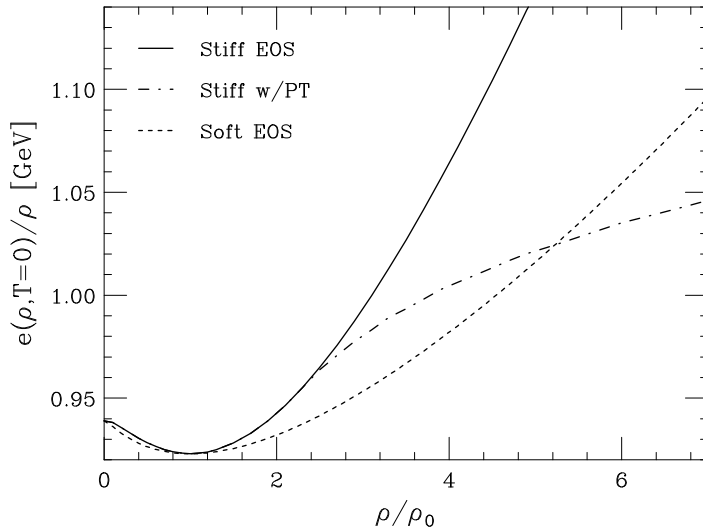


Figure 8. Energy per baryon vs. baryon density, at $T = 0$. Curves are shown for a stiff EOS (solid curve), a soft EOS (dashed), and an EOS with a second-order phase transition (dashed-dot).

To verify whether the expectations regarding the elliptic flow are realistic, we have carried out calculations [8] within a limited version of the transport model based on Eqs. (16) and (18), with nucleon, pion, delta, and N^* degrees of freedom. The mean fields within the model acted on baryons only, giving stiff and soft EOS, at $T = 0$, such as indicated in Fig. 8. We have also carried out the calculations without mean fields. The obtained elliptic-flow excitation functions for Au + Au reactions, at $b = 4 - 6$ fm, are shown in Fig. 9(a). The elliptic flow changes sign from negative values at low beam energies (~ 0.2 AGeV) to positive values at high beam energies (~ 20 AGeV), as expected from the weakening of the squeeze-out contribution to the flow. The energy at which the flow sign changes strongly depends on EOS. Over the range $0.5 \lesssim E_{Beam} \lesssim 10$ AGeV, the dependence on the beam energy is essentially logarithmic. The slope in Fig. 9(a) strongly depends on EOS in accordance with the considerations involving (20). This raises hope that any change in the stiffness of the EOS with energy would be manifested as a change in the slope of the excitation function.

Experience from the low-energy domain ($E_{Beam} \lesssim 1$ AGeV) has shown that the momentum dependence of the mean field is an important factor for the determination of the stiffness of the EOS from flow measurements. Nucleon-nucleus scattering experiments and nuclear-matter calculations clearly indicate the presence of this momentum dependence; in reactions, it plays a role in generating flow before the hadronic matter equili-

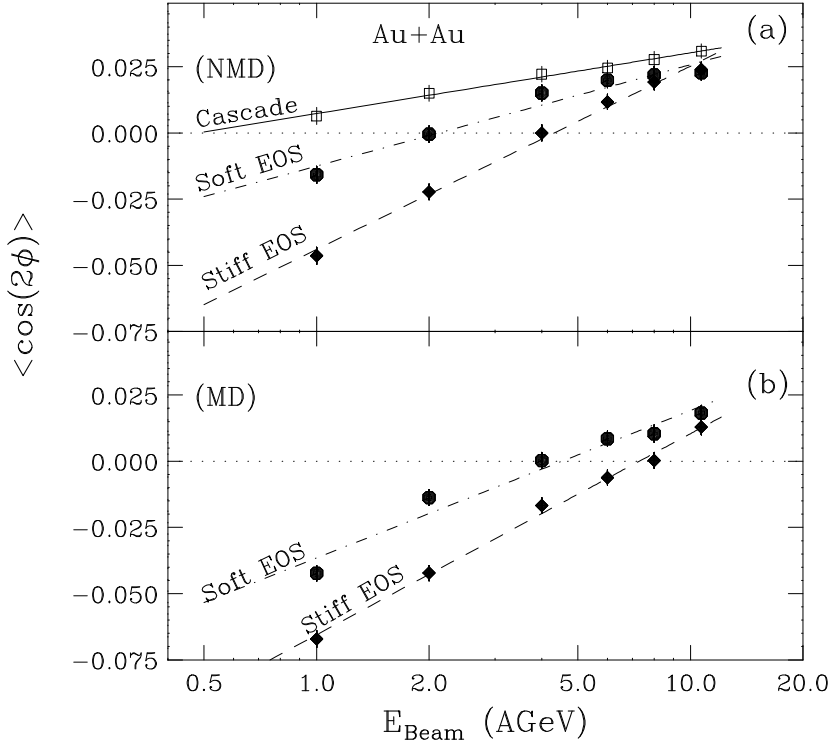


Figure 9. Calculated elliptic flow excitation functions for Au + Au reactions. Panels (a) and (b) show, respectively, the functions obtained without (NMD) and with (MD) the momentum dependent forces. The filled circles, filled diamonds, and open squares indicate, respectively, results obtained using a soft EOS, a stiff EOS, and by neglecting the mean field. The straight lines show logarithmic fits.

brates. A priori, there could be two separate effects due to the momentum dependence: (i) it may pass for an enhanced stiffness of the EOS, and/or (ii) it may lead to a loss of sensitivity to the stiffness of the EOS. The second effect could eliminate the possibility of observing a change in the stiffness with increasing beam energy.

In Fig. 9(b), we show elliptic flow excitation functions obtained from calculations that include momentum-dependent fields acting on the baryons [8]. The general trends of these excitation functions are similar to those shown in Fig. 9(a). However, one can clearly see that the net effect of the momentum dependence is to enhance the squeeze-out. Of greater significance is the fact that the sensitivity of the elliptic flow to the stiffness of the EOS remains practically unchanged when this momentum dependence is included. A cursory examination of Fig. 9 also shows that measurements of elliptic flow should clearly discriminate between models with a realistic EOS and

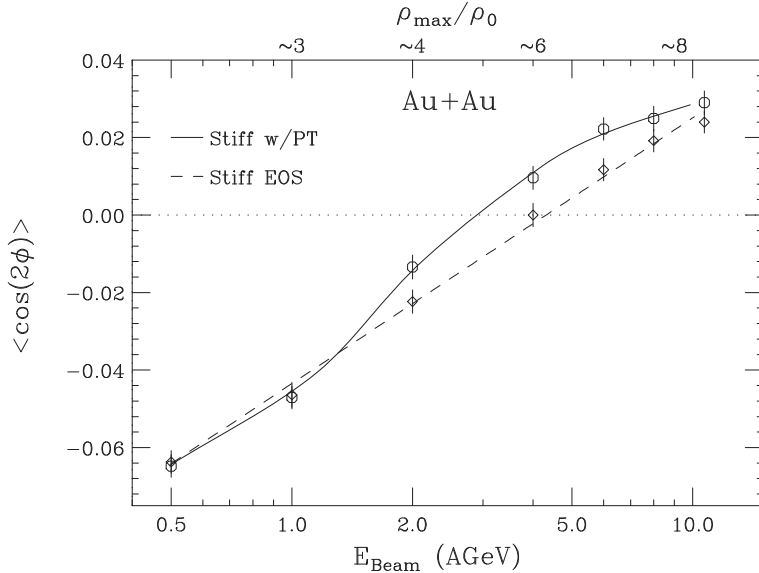


Figure 10. Calculated elliptic flow excitation functions for Au + Au. The open diamonds represent results obtained with a stiff EOS. The open circles represent results obtained with a stiff EOS and with a second-order phase transition. The solid and dashed lines are drawn to guide the eye. Numbers at the top of the figure indicate rough magnitude of local baryon densities reached in reactions at different beam energies.

the cascade model in which the elliptic flow becomes positive right above ~ 0.6 AGeV.

In order to search for an elliptic-flow signature that can signal the onset of a phase transition to the QGP, we have carried out calculations assuming a stiff EOS with a weak second-order phase transition at $\rho_v = 2.3\rho_0$, indicated by the dash-dot line in Fig. 8. The elliptic-flow excitation functions calculated using a stiff EOS with the phase transition (open circles) and a stiff EOS without the phase-transition (diamonds) are compared in Fig. 10. Both functions have been obtained with no consideration of momentum dependence in the mean field. For low beam energies ($\lesssim 1$ AGeV), the elliptic flow excitation functions are essentially identical because the two EOS are either identical or not very different at the densities and temperatures that are reached. For $2 \lesssim E_{\text{Beam}} \lesssim 9$ AGeV the excitation function shows larger in-plane elliptic flow from the calculation which includes the phase transition, indicating that a softening of the EOS has occurred for this beam energy range. This deviation is in direct contrast to the essentially logarithmic beam energy dependence obtained (for the same energy range) from the calculations which assume a stiff EOS without the phase transition. Collection of the data on elliptic flow from EOS, E895, and E877

Collaborations [9] points to a softening at a somewhat higher beam energy, ~ 3 AGeV, than in the reported transport calculations, corresponding to the baryon density $\rho_v \sim 4\rho_0$.

6. Conclusions

To conclude, we have specified a tractable transport model with thermodynamic properties close to those known or expected for the strongly interacting matter. In the phase transition region in the model, along the $\mu = 0$ axis, the masses of elementary excitations drop while the number of active degrees of freedom increases. We have shown that the elliptic flow measurements can discriminate between models with nontrivial EOS and cascade models. The data on the elliptic flow excitation function point to the softening of the EOS in the baryon density region of $\sim 4\rho_0$ ($E_{Beam} \sim 3$ AGeV). These results show a definite need to continue the 1–10 AGeV physics (SIS-AGS). This is the region where crossing of the phase transition may be observed in the excitation functions. These should be established with the best possible accuracy.

Acknowledgements

This work was supported in part by the National Science Foundation under Grant No. PHY-96-05207 and by the U.S. Department of Energy under Contract No. DE-FG02-87ER40331.A008.

References

1. Baym, G., and Chin, S. A. (1976) Landau Theory of Relativistic Fermi Liquids, *Nucl. Phys. A* **262**, p. 527
2. Karsch, F. (1998) On QCD Thermodynamics with Improved Actions, *Nucl. Phys. A Proc. Suppl.* **60**, p. 169
3. Gossiaux, P.-B. and Danielewicz, P. (1998) A Dynamical Effective Model of Ultrarelativistic Heavy Ion Collisions, *Proc. 14th Winter Workshop on Nuclear Dynamics, Snowbird*
4. Ko, C. M., Li, Q. and Wang, R.-C. (1987) Relativistic Vlasov Equation for Heavy Ion Collisions, *Phys. Rev. Lett.* **59**, p. 1084
5. Pang, Y., Schlagel, T. J. and Kahana, S. H. (1993) High Baryon Density from Relativistic Heavy Ion Collisions, *Brookhaven National Laboratory Report BNL-49626*
6. Sorge, H. (1997) Elliptical Flow: A Signature for Early Pressure in Ultrarelativistic Nucleus-Nucleus Collisions, *Phys. Rev. Lett.* **78**, p. 2309
7. Danielewicz, P. (1995) Effects of Compression and Collective Expansion on Particle Emission from Central Heavy-Ion Reactions, *Phys. Rev. C* **51**, p. 716
8. Danielewicz, P., Lacey, R. A. *et al.* (1998) Disappearance of Elliptic Flow: A New Probe for the Nuclear Equation of State, nucl-th/9803047, accepted for Physical Review Letters
9. Pinckenburg, C. *et al.* (1988) Elliptic Flow: A Probe for High Density Nuclear Matter